Chemical Geology 277 (2010) 115–125

Contents lists available at ScienceDirect

Chemical Geology

journal homepage: www.elsevier.com/locate/chemgeo

Solubility of H_2O- and CO_2-bearing fluids in tholeiitic basalts at pressures up to 500 MPa

T.A. Shishkina [a,*], R.E. Botcharnikov [a], F. Holtz [a], R.R. Almeev [a], M.V. Portnyagin [b,c]

[a] Institute of Mineralogy, Leibniz University of Hannover, 30167 Hannover, Germany
[b] Leibniz Institute of Marine Sciences, IFM-GEOMAR, Wischhofstrasse 1–3, 24148 Kiel, Germany
[c] V.I. Vernadsky Institute of Geochemistry and Analytical Chemistry, Kosigin str. 19, 119991, Moscow, Russia

ARTICLE INFO

Article history:
Received 20 October 2009
Received in revised form 12 May 2010
Accepted 28 July 2010

Editor: D.B. Dingwell

Keywords:
H_2O
CO_2
Water
Carbon dioxide
Fluid
Solubility
Tholeiite
Basalt
Magma
Mutnovsky volcano
Kamchatka

ABSTRACT

The solubility of H_2O- and CO_2-bearing fluids in tholeiitic basalts has been investigated experimentally at temperature of 1250 °C and pressures of 50, 100, 200, 300, 400 and 500 MPa. The concentrations of dissolved H_2O and CO_2 have been determined using FTIR spectroscopy with an accurate calibration of the absorption coefficients for hydrogen- and carbon-bearing species using synthesized standards of the same tholeiitic composition. The absorption coefficients are 0.65 ± 0.08 and 0.69 ± 0.08 L/(mol cm) for molecular H_2O and OH groups by Near-Infrared (NIR), respectively, and 68 ± 10 L/(mol cm) for bulk H_2O by Mid-Infrared (MIR). The carbonate groups determined by MIR have an absorption coefficient of 317 ± 23 L/(mol cm) for the band at 1430 cm^{-1}.The solubility of H_2O in the melt in equilibrium with pure H_2O fluid increases from about 2.3 ± 0.12 wt.% at 50 MPa to about 8.8 ± 0.16 wt.% at 500 MPa, whereas the concentration of CO_2 increases from about 175 ± 15 to 3318 ± 276 ppm in the melts which were equilibrated with the most CO_2-rich fluids (with mole fraction of CO_2 in the fluid, $X^{fl}CO_2$, from 0.70 to 0.95). In melts coexisting with H_2O- and CO_2-bearing fluids, the concentrations of dissolved H_2O and CO_2 in basaltic melt show a non-linear dependence on both total pressure and mole fraction of volatiles in the equilibrium fluid, which is in agreement with previous studies. A comparison of new experimental data with existing numerical solubility models for mixed H_2O–CO_2 fluids shows that the models do not adequately predict the solubility of volatiles in basaltic liquids at pressures above 200 MPa, in particular for CO_2, implying that the models need to be recalibrated.
The experimental dataset presented in this study enables a quantitative interpretation of volatile concentrations in glass inclusions to evaluate the magma storage conditions and degassing paths of natural island arc basaltic systems. The experimental database covers the entire range of volatile compositions reported in the literature for natural melt inclusions in olivine from low- to mid-K basalts indicating that most melt inclusions were trapped or equilibrated at intermediate to shallow levels in magmatic systems (<12–15 km).

1. Introduction

Natural subduction-related magmas contain a wide range of volatiles with significant proportions of H_2O and CO_2 as estimated on the basis of volcanic and hydrothermal gas discharges (e.g., Fischer and Marty, 2005). The results of Fischer and Marty (2005) indicate that primitive magmas may contain about 8–16 wt.% H_2O and 3500–7600 ppm CO_2. Evidence for high volatile contents during arc magma genesis and evolution is also given by the analysis of glass inclusions preserved in phenocrysts usually containing up to 6–8 wt.% H_2O and 2500–3000 ppm CO_2 (e.g., Sisson and Layne, 1993; Wallace, 2005). Volcanic gases of typical subduction-related volcanoes have also predominant abundances of H_2O and CO_2 with concentrations varying from ~80 to 99 mol% and from <1 to ~8 mol%, respectively (e.g., Symonds et al., 1994; Giggenbach, 1996). Considering that the solubility of H_2O and CO_2 in silicate melts is mainly dependent on pressure, the concentrations of H_2O and CO_2 determined in glass inclusions and volcanic gasses are commonly used to estimate magma storage conditions and magma evolution history, provided that the volatile solubility data and models are available.

The knowledge on the solubility of H_2O- and CO_2-bearing fluids in silicate melts with compositions ranging from rhyolites to basalts was greatly improved by numerous experimental studies in the last two decades (e.g., Blank et al., 1993; Blank and Brooker, 1994; Dixon et al., 1995; Jakobsson, 1997; Tamic et al., 2001; King and Holloway, 2002; Behrens et al., 2004a; Botcharnikov et al., 2005a, 2006). Based on the experimental datasets, several empirical and semi-empirical (thermodynamic) models have been proposed as tools to reconstruct magma degassing conditions (e.g., Dixon et al., 1995; Papale, 1999; Tamic et al.,

* Corresponding author. Institute of Mineralogy, Leibniz University of Hannover, 30167 Hannover, Germany, Callinstr. 3. Tel.: +49 511 762 4753; fax: +49 511 762 3045.
E-mail address: t.shishkina@mineralogie.uni-hannover.de (T.A. Shishkina).

0009-2541/$ – see front matter © 2010 Elsevier B.V. All rights reserved.
doi:10.1016/j.chemgeo.2010.07.014

2001; Newman and Lowenstern, 2002; Behrens et al., 2004a; Liu et al., 2005; Papale et al., 2006). However, our understanding of mixed H_2O and CO_2 volatile solubilities in typical basaltic magmas is limited by the very few available experimental data. Furthermore, published datasets are restricted to pressures <200 MPa (Dixon et al., 1995; Botcharnikov et al., 2005a) and are only useful to model relatively shallow depths of magma degassing. The composition of a fluid phase, coexisting with an ascending magma body may change significantly during magma ascent as a result of a strong dependence of volatile solubilities on pressure and fluid composition (e.g., the solubility of H_2O is two orders of magnitude higher than that of CO_2). The volatile solubility extrapolations up to pressure of 500 MPa in the recent models of Newman and Lowenstern (2002) and Papale et al. (2006) are only weakly supported by the experiments, making estimates of degassing conditions for typical basaltic magmas inaccurate. A large and growing database of volatile concentration measurements in glass inclusions (in particular of basaltic composition) obviously requires additional experimental data at high pressures and temperatures to better constrain degassing conditions of natural magmas.

Here we present new experimental data on the solubility of H_2O and CO_2-bearing fluids in basaltic magmas of Mutnovsky volcano, Kamchatka, Russia. Based on their major element composition, the erupted lavas of Mutnovsky are typical island arc high-Al, low-K tholeiitic basalts (Martynov and Chashchin, 1989; Martynov et al., 1995; Pineau et al., 1999; Duggen et al., 2007). The solubility data are obtained for pressures from 50 to 500 MPa, covering the wide range of typical pressures/depths of glass inclusion entrapment, and are useful for quantitative evaluation of magma storage conditions and degassing of natural basaltic magmas.

2. Experimental and analytical methods

2.1. Starting materials and capsule preparation for solubility experiments

The experiments on solubility of H_2O and CO_2 in basaltic melt were conducted using natural basalt from Mutnovsky volcano (sample N72 from Duggen et al., 2007). This sample is the most primitive basalt of the rocks collected at Mutnovsky volcano (see composition in Table 1). It is composed of phenocrysts of plagioclase and olivine distributed in a fine-grained groundmass consisting of plagioclase, clinopyroxene and magnetite. The sample was powdered and melted for 3 h in a Pt-crucible in an oven at 1600 °C and 1 atm, then rapidly quenched to a glass. This glass was crushed and the same melting procedure was repeated for 1.5 h. The major element composition and homogeneity of the finally quenched basaltic glass were inspected by electron microprobe analysis (Table 1). The basaltic glass was crushed and sieved into two fractions: <125 μm and 125–200 μm. Before loading into capsules, these fractions were mixed in proportion ~1:1 to minimize the free volume between grains and hence, the incorporation of atmospheric nitrogen.

$Au_{80}Pd_{20}$-capsules with a diameter of 2.6–3.4 mm, a length of 15–20 mm were used to conduct the experiments on volatile solubility. About 50 mg of basaltic glass powder was placed in each capsule. Distilled water (0–8 μl H_2O) and $Ag_2C_2O_4$ (0–15 mg) were used as sources of H_2O and CO_2, respectively. Water and silver oxalate were loaded into the capsules in different proportions to establish different mole fractions of water in the added fluid phase (XH_2Oin) before experiment (Table 2). Capsules were weighed after loading of each component. Capsules were closed with pliers and cooled using liquid nitrogen to avoid loss of water and CO_2 during welding. After welding, the capsules were checked for leakage by heating in a drying furnace for at least 1 h at 110 °C and consequent weighing.

It must be noted that in this study the concentration of water and especially carbon-bearing species in the quenched glasses were determined using infrared spectroscopy. Considering that the main source of error on the absolute concentrations of water- and carbon-bearing species is related to uncertainties on the absorption coefficients (e.g., Ohlhorst et al., 2001), we synthesized four large (~500 mg) samples to determine the absorption coefficients for the basaltic composition used in this study (in particular the absorption coefficient for carbonate groups in the glasses). The $Au_{80}Pd_{20}$-capsules (diameter 5 mm, length 35 mm) were filled with 500 mg of basaltic glass powder, 5–30 μl of H_2O, 1.5–3 mg $Ag_2C_2O_4$ or 1–3 mg $CaCO_3$. To achieve homogenous distribution of the components, the capsules were filled in several steps (water and silver oxalate were added as small portions at different levels of the capsule). When $CaCO_3$ was used as a source of CO_2, it was mixed with basalt glass powder before loading.

Table 1
Composition of starting material in wt.% (sample N72, basalt from Mutnovsky volcano), recalculated to 100 wt.%.

	SiO_2	TiO_2	Al_2O_3	FeO-t	MnO	MgO	CaO	Na_2O	K_2O	P_2O_5
1	50.07	0.90	18.36	9.35	0.17	7.02	11.32	2.45	0.22	0.15
2	50.17	0.92	18.28	9.37	0.17	7.00	11.37	2.33	0.23	0.15

Notes:
1 – XRF data (wt.%) for natural sample after Duggen et al. (2007).
2 – average of 50 microprobe measurements for the remelted sample used in the experiments.

2.2. Experimental technique

We used a vertically oriented internally heated pressure vessel (IHPV) with Ar as pressure medium. The temperature in the IHPV was recorded with four unsheathed S-type ($Pt–Pt_{90}Rh_{10}$) thermocouples with a temperature gradient along the sample of ±3 °C. Total pressure was recorded continuously with a calibrated Burster Type 8221 digital pressure transducer (pressure uncertainty ±1 MPa). The variation of pressure during the experiments did not exceed 5 MPa. Several sets of experiments were performed at the same temperature of 1250 °C and at pressures of 50, 100, 200, 300, 400 and 500 MPa. Five to six capsules with different proportions of H_2O and CO_2 (XH_2Oin from 0 to 1, Table 2) were placed in the pressure vessel for each experiment. The duration of each run was about 24 h. The samples were quenched isobarically with a quench rate of about 150 °C/s using a rapid-quench technique described by Berndt et al. (2002). The intrinsic redox conditions in the IHPV ($fO_2^{intrinsic}$) at $aH_2O = 1$ are close to $\log fO_2 = NNO + 2.6$ (the oxygen fugacity is higher than that buffered by the Ni/NiO assemblage by 2.6 orders of magnitude) according to the recent determinations reported by Schuessler et al. (2008). The oxygen fugacity prevailing in each individual capsule is dependent on water activity because it is controlled by the equilibrium reaction of water dissociation ($H_2 + 1/2\ O_2 = H_2O$) inside the capsules. Water activities for every run were calculated from the composition of the fluid phase ($X^{fl}H_2O$, see Section 2.3) using activity coefficients after Aranovich and Newton (1999) and molar volumes of pure H_2O after Pitzer and Sterner (1994). The fO_2 was calculated for each experiment using the expression $\log fO_2^{capsule} = \log fO_2^{intrinsic} + 2\log(aH_2O)$ (see also Botcharnikov et al., 2005b) and the calculated values for each experiment are reported in Table 2.

Experiments designed for the determination of molar absorption coefficients (preparation of reference glasses) were carried out at 1250 °C and 500 or 300 MPa for 24 h followed by rapid quench.

2.3. Determination of fluid composition after experiment

A conventional weight-loss procedure was employed for determination of the mole fractions of H_2O ($X^{fl}H_2O$) and CO_2 ($X^{fl}CO_2$) in the fluid phase after experiment. Capsules were weighed after the runs and cooled by putting them into liquid nitrogen to freeze H_2O in the fluid phase. Frozen capsules were punctured with a steel needle and

Table 2
Experimental conditions and results of Karl–Fischer titration, determinations of redox state of Fe and infrared spectroscopy.

Capsule NN	P (MPa)	$XH_2O in$ [a]	$X^{fl}H_2O$ [b]	ΔNNO[c]	H_2O (wt.%) KFT[d]	FeO loss, % relative [e]	Fe(II)/Fe total [f]	H_2O-t, wt.% (3550 cm^{-1}) MIR [g]	H_2O-m, wt.% (5200 cm^{-1}) NIR	OH, wt.% (4500 cm^{-1}) NIR	H_2O total, wt.%, NIR [h]	CO_2, ppm (1430 cm^{-1}) (MIR)
M13	50	1.00	1.00 (8)	2.60	1.67 (14)	–	n.a.	n.a.	n.a.	n.a.	–	0
M14	50	0.93	1.00 (5)	2.60	1.82 (12)	–	0.64 (2)	1.59 (21)	0.59 (6)	1.12 (12)	1.71 (13)	0
M15	50	0.78	0.48 (8)	2.00	1.54 (12)	–	0.68 (2)	1.43 (20)	0.54 (6)	0.98 (10)	1.52 (12)	60 (7)
M16	50	0.54	0.20 (8)	1.28	1.07 (12)	6.55	0.73 (2)	1.10 (17)	n.a.	n.a.	–	92 (8)
M51	50	0.94	0.98 (3)	2.58	2.24 (11)	–	0.66 (3)	n.a.	0.96 (10)	1.38 (14)	2.34 (17)	0
M50	50	0.83	0.67 (6)	2.27	2.43 (12)	–	0.70 (2)	n.a.	0.73 (8)	1.17 (13)	1.90 (15)	35 (3)
M49	50	0.52	0.31 (8)	1.64	1.25 (12)	6.04	0.75 (2)	n.a.	0.44 (5)	0.79 (8)	1.23 (10)	114 (10)
M48	50	0.00	0.20 (8)	1.24	0.77 (11)	12.47	0.79 (2)	0.70 (13)	0.34 (4)	0.51 (5)	0.85 (6)	176 (15)
M47	50	0.00	0.18 (8)	1.20	0.82 (12)	10.60	0.75 (2)	0.73 (12)	0.34 (4)	0.51 (5)	0.85 (7)	175 (14)
M6	100	1.00	1.00 (5)	2.60	2.80 (13)	–	0.64 (2)	n.a.	1.46 (16)	1.68 (17)	3.14 (23)	0
M7	100	0.94	0.60 (8)	2.18	2.97 (12)	–	0.66 (2)	n.a.	1.49 (15)	1.60 (16)	3.08 (22)	0
M8	100	0.77	0.49 (5)	2.02	2.26 (12)	–	0.71 (2)	2.06 (23)	0.94 (10)	1.27 (13)	2.21 (17)	157 (13)
M9	100	0.38	0.12 (6)	0.87	1.20 (12)	13.33	0.84 (2)	1.31 (20)	0.00	0.78 (9)	0.78 (9)	292 (24)
M10	100	0.00	0.08 (5)	2.60	0.75 (11)	16.84	0.88 (3)	0.84 (17)	0.00	0.55 (6)	0.55 (6)	341 (27)
M11	200	1.00	1.00 (3)	2.60	4.95 (12)	–	0.56 (2)	n.a.	2.92 (30)	2.06 (21)	4.98 (37)	0
M12	200	0.94	0.88* (5)	2.49	4.44 (13)	–	0.57 (2)	n.a.	2.31 (24)	1.91 (20)	4.22 (31)	195 (18)
M2	200	0.89	0.63 (4)	2.23	4.22 (13)	–	0.82 (3)	n.a.	2.09 (22)	1.88 (20)	3.97 (30)	296 (24)
M3	200	0.78	0.47 (5)	2.01	3.21 (14)	–	0.65 (3)	n.a.	1.36 (14)	1.65 (17)	3.00 (22)	598 (48)
M5	200	0.00	0.06 (5)	0.31	0.64 (13)	12.53	0.88 (3)	0.82 (17)	0.00	0.52 (5)	0.52 (5)	990 (83)
M33	300	1.00	1.00 (2)	2.60	6.25 (12)	–	n.a.	n.a.	4.16 (43)	2.23 (23)	6.39 (48)	0
M34	300	0.95	0.87 (3)	2.49	5.70 (13)	–	0.57 (2)	n.a.	3.62 (38)	2.22 (23)	5.84 (44)	375 (30)
M35	300	0.84	0.57 (4)	2.17	4.20 (12)	–	0.61 (2)	n.a.	2.28 (23)	1.94 (20)	4.23 (31)	1019 (81)
M36	300	0.71	0.34 (5)	1.78	2.82 (11)	–	0.66 (2)	n.a.	1.44 (15)	1.61 (17)	3.05 (22)	1392 (111)
M37	300	0.00	0.05 (5)	0.19	0.65 (12)	26.72	0.79 (3)	0.48 (9)	0.27 (3)	0.26 (3)	0.53 (4)	1627 (142)
M38	400	1.00	1.00 (5)	2.60	7.36 (12)	–	0.54 (2)	n.a.	n.a.	n.a.	–	0
M39	400	0.96	0.89 (3)	2.51	6.75 (12)	–	0.54 (2)	n.a.	4.59 (47)	2.30 (24)	6.89 (52)	681 (54)
M30	400	0.88	0.67 (4)	2.30	5.65 (12)	–	0.59 (2)	n.a.	3.22 (34)	1.97 (21)	5.18 (39)	1271 (101)
M40	400	0.63	0.31 (4)	1.73	3.07 (12)	–	0.64 (2)	n.a.	1.43 (15)	1.60 (16)	3.03 (22)	2183 (178)
M19	500	0.64	0.18 (4)	1.45	3.29 (13)	–	0.70 (2)	n.a.	1.49 (15)	1.68 (17)	3.16 (23)	3277 (266)
M20	500	0.87	0.64* (5)	2.28	5.72 (12)	–	0.61 (2)	n.a.	3.73 (38)	2.19 (22)	5.91 (44)	2421 (268)
M21	500	0.97	0.91* (5)	2.52	7.56 (14)	–	0.56 (2)	n.a.	n.a.	n.a.	–	1051 (98)
M22	500	1.00	1.00 (6)	2.60	8.81 (16)	–	0.54 (2)	n.a.	n.a.	n.a.	–	0
M42	500	0.23	0.07 (3)	0.55	1.33 (11)	5.44	0.75 (2)	1.42 (19)	0.69 (8)	0.96 (11)	1.65 (13)	3318 (276)
M43	500	0.52	0.16 (4)	1.24	2.62 (11)	–	0.67 (2)	n.a.	1.24 (13)	1.55 (16)	2.79 (21)	3172 (265)
M44	500	0.73	0.27 (5)	1.65	4.00 (12)	–	0.63 (2)	n.a.	2.20 (23)	1.91 (19)	4.11 (30)	3029 (244)
M46	500	0.91	0.76* (5)	2.39	6.69 (12)	–	0.57 (2)	n.a.	4.80 (49)	2.28 (23)	7.09 (55)	2189 (181)

Notes:
n.a. – was not analyzed; calculated errors are shown in brackets near values (1σ deviation).
[a] Mole fractions of H_2O in fluid loaded to the capsules before experiments.
[b] Mole fractions of H_2O in fluid in the capsules after experiments, * – values calculated by mass-balance when weight-loss procedure failed.
[c] Deviation of oxygen fugacity from Ni/NiO buffer in log units (calculation procedure described in Section 2.2).
[d] KFT represents a single measurement with error calculated by error propagation considering errors in titration rate of 0.02 mg/s, errors in sample weight of 0.1 mg, and uncertainty of unextracted water of 0.10 wt.%.
[e] Deviations of FeO-total concentrations in experimental glasses from initial composition (Table 1), only deviations higher then ±5% relative are shown.
[f] 2σ error (calculated from analytical uncertainties) is shown.
[g] Errors of the calculated concentrations of H_2O and CO_2, determined by IR, calculated by error propagation considering errors of thickness (0.0002 cm), density (2% relative). reproducibility of absorbance (for each band respectively) and errors of the absorption coefficients (from Table 3).
[h] Sum of H_2O-molecular and OH-group concentrations determined by near-infrared spectroscopy.

warmed up to room temperature. By subsequent weighing, the mass of CO_2 in the fluid was determined. The capsules were then placed into an oven at 110 °C for 2–3 min (500 MPa-runs were held at 60 °C) and weighed to determine the mass of evaporated H_2O. Weighing was repeated until no loss of water was detected anymore. It can be noted that the technique to determine the mass of free CO_2 in the capsule does not discriminate between CO_2 and N_2. An entrapment of atmospheric nitrogen in the experimental charge during loading the capsules was estimated to be small (0.5 to 4 mol%, Tamic et al., 2001). As a main source of errors for the determined mole fractions of H_2O and CO_2 in the fluid we considered the uncertainty in the weighing of the capsules before and after piercing (0.1 and 0.05 mg for CO_2 and H_2O, respectively). Additional uncertainty, induced by atmospheric nitrogen, was taken into account (0.007 mol% for H_2O and 0.02 mol% for CO_2, according to (Tamic et al., 2001).

In capsules for which the weight-loss procedure of determining the fluid composition failed, the mole fractions of H_2O and CO_2 in fluid were calculated by mass-balance using initial amounts of loaded volatiles and rock powder and measured concentrations of volatiles in run-product glasses (see Table 2). The data obtained by mass balance have a higher uncertainty, especially because the system is not closed for hydrogen during the experiments.

2.4. Water determination by Karl–Fischer titration

The determination of H_2O dissolved in the glasses was made by Karl–Fischer titration (KFT, Behrens et al., 1996). The samples (composed of one or several glass pieces with a total weight of about 10–20 mg) were placed into an open platinum crucible and heated up with a high-frequency generator (Linn electronic HTG 1000/1,3) from room temperature to 1300 °C. Extracted water was transported by an Ar-stream to the titration cell with an electrolytic solution. The amount of extracted H_2O was measured by a moisture meter (Mitsubishi CA-100) after quantitative reaction between H_2O and coulometrically generated I_2. The uncertainty in the water determination was estimated on the basis of the uncertainty of the titration rate which is 0.2 μg/s (Behrens et al., 1996). Behrens et al. (1996) noted that there is always ~0.1 wt.% unextracted water in the

glasses after heating and corrected the water concentration in the glass by adding this value. However, this observation was made for feldspatic glasses. Considering that water diffusivity is higher in basaltic melts compared to that in more silicic melts (Behrens et al., 2004b), a more effective extraction can be expected in our glasses. Thus, instead of a correction of the KFT data, an additional uncertainty of ± 0.1 wt.% was considered in the error calculation. The results were also used for the calibration of IR absorption coefficients.

2.5. Determination of total dissolved carbon in reference glasses

For the calibration of IR absorption coefficients for carbon-related bands in glasses, the total carbon content in glasses needs to be analyzed. The total carbon concentration in the reference glasses was analyzed by combustion and subsequent IR spectroscopy using an ELTRA CS 800 analyzer. For each measurement about 100 mg of basaltic glass was loaded into a corundum crucible together with ~1.5 ± 0.05 g W and 0.3 ± 0.03 g Fe. The mixture was fired in an oxygen stream at temperature up to 2200 °C (according to the manufacturer). After combustion, the released CO_2 was measured in an IR cell.

For calibration of the method, background measurements and analyses using metallic and glass standards with known carbon contents were performed. In the background measurements, a corundum crucible was loaded with W and Fe without any sample and an average value of 5.1 ± 0.4 μg C was determined. The air-melted starting glass was analyzed and the average of three measurements yielded a carbon concentration of 8.2 ± 1.4 μg C (about 0.009 wt.% CO_2). The concentrations of total carbon in the four glasses synthesized as reference materials were found to be 691 ± 11 (St-1), 1136 ± 74 (St-2), 1394 ± 125 (St-3) and 871 ± 16 (St-6) ppm CO_2 (water concentrations are 2.96 ± 0.09, 2.84 ± 0.05, 1.33 ± 0.04 and 1.58 ± 0.09 wt.%, respectively).

2.6. Fourier-transform infrared spectroscopy (FTIR)

Water and carbonate concentration in basaltic glasses were calculated using IR-spectra of absorption on the basis of the Beer–Lambert law:

$$C_i = 100^* M_i^* A_j / \left(d^* \rho^* \varepsilon_j\right) \quad (1)$$

where C_i is the concentration of species in wt.%, M_i is the molecular weight of the species, A_j is the absorbance (peak height) of band j, d is the thickness of the section, ρ is the density in g/L and ε_j is the absorption coefficient of band j in L/(mol cm).

The concentrations of water- and carbon-bearing species dissolved in basaltic glass were determined from absorption spectra using a Bruker IFS88 FTIR spectrometer combined with an IR-ScopeII microscope (Institute of Mineralogy, Hannover). The bands of interest are in the mid-infrared (MIR) and near-infrared (NIR) range. The operating conditions for MIR were: globar light source and KBr beamsplitter, spectral resolution 2 cm^{-1}; for NIR–W-lamp and CaF_2 beamsplitter, spectral resolution 4 cm^{-1}. A MCT narrow range detector was used for both MIR and NIR. The microscope and the sample were flushed with dry air to minimize the effect of atmospheric carbon dioxide on CO_2 content of the glasses (Tamic et al., 2001). The glasses were prepared as both-side polished thin sections with a thickness of ~100 μm for MIR and ~250 μm for NIR. For each spectrum 50 to 100 scans were collected from spots with sizes of about 50*50 μm. For every sample 3 to 5 spectra were collected in different parts of the glass piece to check for homogeneity of volatile distribution.

The thickness of the polished pieces of glass was measured with a digital micrometer Mitutyo (precision ± 2 μm (Behrens et al., 2009) in 5 points. It was not possible to measure the density of each experimental sample because of the small size of the glass pieces. Densities were calculated using the density of the water-free starting basaltic glass (composition given in Table 1) and assuming a partial molar volume of H_2O in the glass of 12.0 ± 0.5 cm^3/mol (Holtz et al., 1995; Richet et al., 2000). The density of the water-free glass was determined to be 2757 ± 3 g/l after weighing two glass pieces (640 and 1300 mg) in water and in air. The densities of hydrous glasses can be calculated using following equation:

$$\rho = (2757 - 22.1^* H_2O) \quad (2)$$

where H_2O is the water content in wt.%. The uncertainty on density values calculated following this procedure is estimated to be about ±2 rel.% (Behrens et al., 2009). Density variations due to pressure can be neglected (Behrens et al., 2009) and were not taken into account.

2.7. Electron microprobe

Major-element composition of the air-melted starting glass and experimental products were analyzed by electron microprobe (Cameca SX100). Conditions of measurements were 15 keV accelerating voltage, 4 nA beam current, 20 μm diameter of electron beam. Sodium and potassium were analyzed first to minimize alkali-loss. Cameca standards were used for calibration. The composition of the starting glass is an average value of 50 analyses (Table 1). For all other glasses, 5 to 10 different points were analyzed to check for the homogeneity of samples and to improve reproducibility.

2.8. Wet-chemical colorimetric method for determination of redox state of Fe

The analytical approach for the determination of ferrous Fe in experimental silicate glasses is based on the analytical technique of Wilson (1960) modified by Schuessler et al. (2008) to minimize the use of toxic materials. The analytical method was optimized to measure the Fe^{2+}/Fe-total ratio of milligram-sized samples. The accuracy and precision was tested with international reference materials and with standards analyzed by other methods. The replicate measurements for different rocks and minerals containing between 1 and 8 wt.% ferrous Fe showed that the precision of Fe^{2+}/Fe-total determination using this technique is within ± 0.03 (2σ). Based on the calibration, it was concluded that this method can be reliably applied for silicate glasses with Fe^{2+}/Fe-total ratios in the range from 0.4 to 0.9 (Schuessler et al., 2008). Three to six milligrams of glasses from our samples were measured, applying this technique. The errors of the Fe^{2+}/Fe-total determination include analytical uncertainty of the method (arise mainly from the spectroscopic measurements, Table 2).

3. Results

3.1. Experimental products and glass composition

The experimental conditions and the analytical results are reported in Table 2. The experiments were carried out at a temperature higher than the liquidus and most experimental products are composed of quenched brown bubble- and crystal-free glasses, coexisting with a fluid phase (as determined by weight-loss). In one sample (M22, run at 500 MPa and $XH_2O in = 1$) we observed some rare elongated needle-like crystals. This sample has the highest water content and the observed crystals may have formed during quench due to enhanced kinetics of crystallization in H_2O-rich melts. For this sample the water concentrations were not determined by IR spectroscopy since the presence of crystals in the glass may affect the quality of IR measurements.

In most cases, the major-element compositions of glasses do not differ significantly from the composition of the initial glass. Deviations from starting composition for SiO_2, Al_2O_3, MgO, CaO, TiO_2 are within

±3% relative (loss of Fe in some runs is discussed below) if normalized to volatile-free basis (see Tables A1, A2 in electronic supplementary information), showing that the incongruent dissolution of melt components in the fluid can be neglected (the amount of melt dominates over that of fluid). IR spectroscopic data demonstrate homogeneous distribution of H_2O and CO_2 in all glasses, indicating that run duration was long enough to reach equilibrium between fluid phase and melt.

Water was detected in all samples, even in experiments with initial $XH_2O in = 0$ (no H_2O was loaded in the capsule). This is related to the reduction of the melt in the high pressure experiments when compared to the starting melt composition (synthesized at oxidizing atmospheric conditions). In the presence of small amounts of hydrogen in the pressure vessel (hydrogen diffuses through the noble metal capsules at high temperature), the reduction of glasses results in the formation of water, presumably according to the reaction $Fe_2O_3 + H_2 = 2FeO + H_2O$. Thus, in the nominally dry samples, small amounts of water were generated in the capsules. The determination of the FeO/FeOtotal ratios in the glasses confirm (1) that the glasses are more reduced after the experiments and (2) that there is an increasing amount of Fe^{3+} with increasing amount of added water (Table 2). The initial FeO/FeOtotal ratio in the starting composition was ~0.45 (about 4 wt.% FeO and 5 wt.% Fe_2O_3), whereas after the experiments this ratio varied from 0.54 in the most oxidized glasses (samples with $XH_2O in = 1$) to 0.88 in the most reduced samples (samples with $XH_2O in = 0$).

In addition to a change of the redox state, a noticeable loss of Fe from the glass into $Au_{80}Pd_{20}$ capsules was observed in the six most reduced glasses performed with $XH_2O in = 0$ (Table 2). In those experiments, the relative loss of Fe (compared to the composition of the starting glass) was found to be 10 to 16% relative in four experiments and 27% relative in the experiment M37. For most glasses with $XH_2O in > 0$, the Fe loss is negligible (FeO is identical to that of the starting glass within the error of the electron microprobe measurements for hydrated silicate glasses) and always <6.5% relative, except for experiment M9 (Table 2). Such change in the redox state of iron and in the melt composition (for nominally dry experiments) may potentially affect the concentrations of dissolved H_2O and CO_2.

3.2. Determination of IR absorption coefficients

Typical MIR and NIR spectra used to determine the CO_2 and H_2O concentrations are shown in Fig. 1 (data at 500 MPa). It can be noted that carbon is dissolved as carbonate only, in agreement with previous observations made for basaltic compositions (e.g., Fine and Stolper, 1986; Blank and Brooker, 1994; Dixon et al., 1995; Botcharnikov et al., 2005a). Using the data obtained from the bulk analysis (CS) of dissolved carbon in the four reference glasses and using the KFT data obtained for the whole dataset, linear molar absorption coefficients (ε) were calculated for every IR band of interest by regression of absorbance (normalized by density and section thickness) against the total water or carbon concentrations in glasses determined with independent methods (Table 3). The absorbance for NIR bands was always determined using linear baselines (Fig. 1b). The intensity of carbonate bands and of the MIR water band was determined by first subtracting a spectrum of volatile-free glass (starting material) scaled to the same thickness and then drawing a linear baseline below the carbonate and the water bending vibration bands as shown in Fig. 1a (see also Behrens et al., 2009). In this work carbonate concentrations in the glasses were quantified using the peak height of the 1430 cm^{-1} band, because the band at 1520 cm^{-1} is partly superimposed with that of the molecular water at 1630 cm^{-1}. This effect results in increasing A_{1520}/A_{1430} value with increasing total water content in the glass, as already shown by Botcharnikov et al. (2006) and Behrens et al. (2009) for andesitic and phono-tephritic compositions, respectively.

Using the available dataset, the regression between the absorbances for bands at 4500 and at 5200 cm^{-1} (normalized by density, thickness and water content from KFT measurements), was evaluated in order to determine the absorption coefficients of water species in the glasses (see Fig. 2a). The absorption coefficients for the bands at 4500 cm^{-1} and at 5200 cm^{-1} are found to be equal to 0.69 ± 0.08 and 0.65 ± 0.08 L/mol cm, respectively (Fig. 2a). These data are in a good agreement with observations on the effects of melt composition on the absorption coefficients (e.g., Ohlhorst et al., 2001; Mandeville et al., 2002; Behrens et al., 2009), indicating that approximately identical values should be expected for both the 4500 cm^{-1} and the 5200 cm^{-1} bands. In addition, our data are identical within error with those of MORB compositions determined by Dixon et al. (1995). The absorption coefficient for the band at 3550 cm^{-1} can be determined from an average of individual coefficients using each data point. In this case, the average absorption coefficient is 68 ± 10 L/mol cm. The absorption coefficient can also be calculated using a regression of the absorbance (normalized by density and thickness) vs. water concentration determined by KFT in experimental and standard glasses (Fig. 2b). In this case, a value of 65 ± 2 L/mol cm is obtained. Although both values are identical within uncertainty, the second value is in better agreement with the data published previously by Dixon et al. (1995; 63 ± 3 L/mol cm). For carbonate, four samples could be used for the calibration of the absorption coefficient and a value of 316 ±

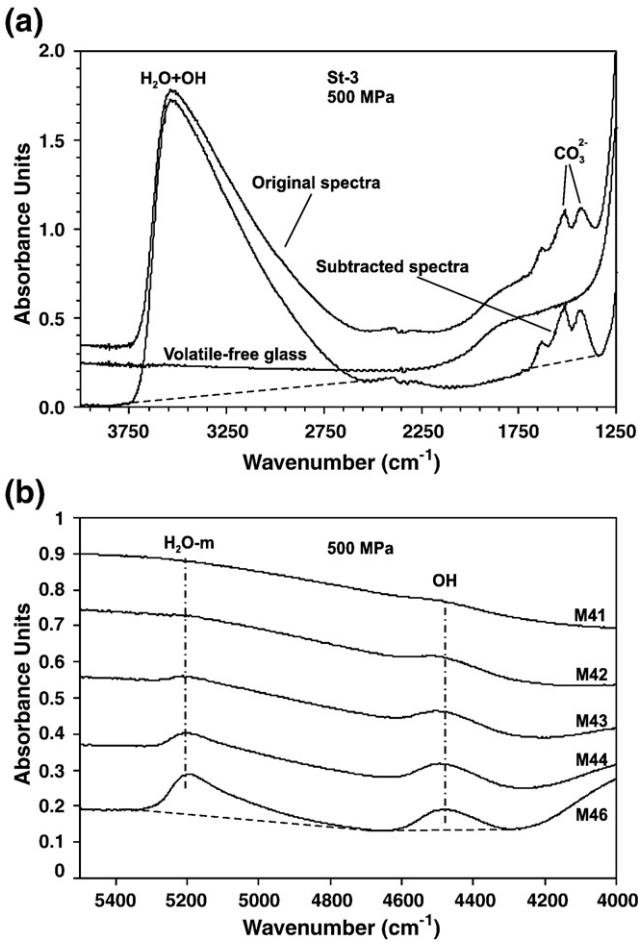

Fig. 1. Infrared spectra of experimental glasses. (a) Typical mid-infrared (MIR) spectrum of H_2O- and CO_2-bearing glass (St-3, $P = 500$ MPa; upper solid line), dry starting glass (thick solid line) and spectrum obtained by subtraction of a spectrum of volatile-free glass from that of the sample after normalization to the same thickness. Dashed lines are baselines that were used for measuring peaks heights for 3550 cm^{-1} and 1430 cm^{-1} bands. (b) Series of near-infrared (NIR) spectra (solid lines) of experimental glasses with different water concentrations after experiment at 500 MPa (see Table 2). Dashed-dotted lines show position of 4550 cm^{-1} (OH-group) and 5200 cm^{-1} (H_2O-molecular) bands. Dashed lines are baselines used for measuring band intensities.

Table 3
Linear molar absorption coefficients.

	Species	ε [L/mol cm] (linear regression)	ε [L/mol cm] (average)	Range of H_2O^{tot} (wt.%)
ε_{1430}	Carbonate	316 ± 12	317 ± 23	1.33–2.96
ε_{3550}	OH, H_2O-m	65 ± 2	68 ± 10	0.28–2.26
ε_{4500}	OH	0.69 ± 0.08		0.28–6.75
ε_{5200}	H_2O-m	0.65 ± 0.08		0.28–6.75

Notes:
Molar absorption coefficients for carbonate band (1430 cm^{-1}) were calculated using standard glasses. For other bands the determination was performed by using dataset of experimental and standard glasses. Molar absorption coefficients for carbonate (1430 cm^{-1}) and water (3550 cm^{-1}) were calculated using two ways: 1) by averaging individual coefficients, calculated for each data point (average) and 2) by regression of absorbance normalized by density and section thickness against the total carbon or water concentrations in glasses determined by independent methods (linear regression). In this work, for calculations of CO_2 and H_2O concentrations in experimental glasses with 1430 cm^{-1} and 3550 cm^{-1} bands, respectively, linear molar absorption coefficients determined by averaging were used (see Section 3.2). Errors for average values represent 1 standard deviation, for linear – 3σ-deviations determined from linear regression.

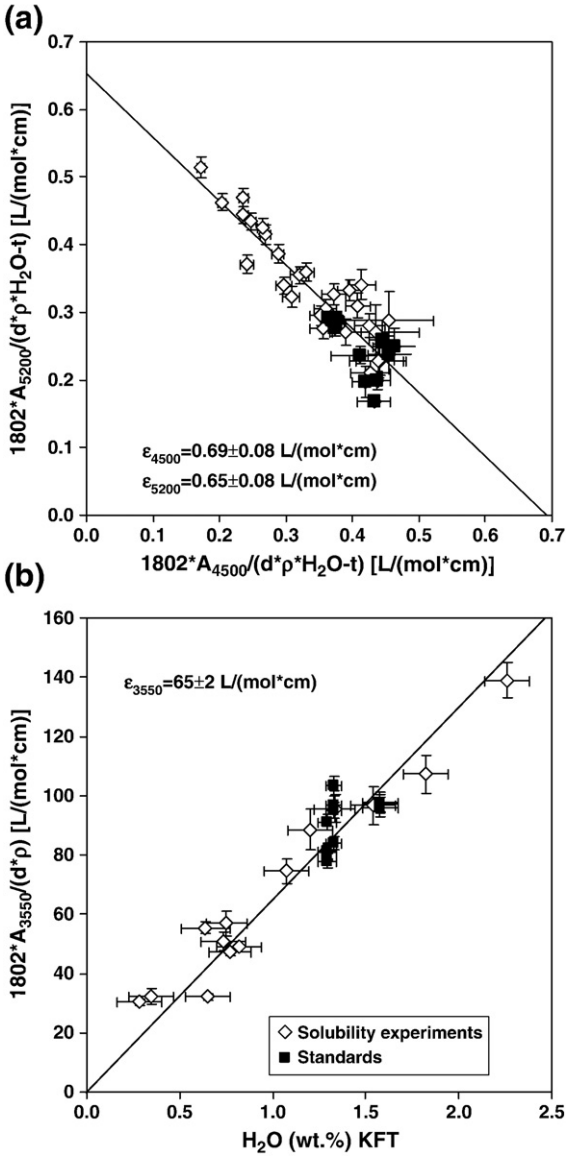

Fig. 2. (a) Calibration plot for the determination of the absorption coefficients for the 4550 cm^{-1} and 5200 cm^{-1} bands. (b) Plot of normalized absorbance of the 3550 cm^{-1} band vs. water concentration in the glasses determined by KFT (see Section 3.2).

12 L/mol cm was determined with the slope of the normalized absorbance at 1430 cm^{-1} vs. CO_2 tot (Fig. 3). A similar value was obtained by averaging the ε_{1430} values determined for each section separately: 317 ± 23 L/mol cm. This value is lower by 15% relative than that proposed by Fine and Stolper (1986; 375 ± 20 L/mol cm) for a tholeiitic composition. In this study we used the values of 317 ± 23 (ε_{1430}) and 68 ± 10 L/mol cm (ε_{3550}) for the calculation of CO_2 and total water concentrations in the glasses, respectively.

3.3. Concentrations of water and CO_2 in coexisting fluids and glasses

The concentrations of H_2O and CO_2 dissolved in glasses as a function of the fluid phase composition are shown in Fig. 4. In general, water and CO_2 concentrations increase non-linearly with increasing mole fraction of these components in the coexisting fluid ($X^{fl}H_2O$ and $X^{fl}CO_2$, respectively).

In glasses which are in equilibrium with pure H_2O-bearing fluid, the amount of dissolved water increases from about 2.3 wt.% at 50 MPa to 8.8 wt.% at 500 MPa (Fig. 5a). At low pressures (<200 MPa), the dependence of water solubility on pressure can be generally described as a power function, and at higher pressures the trend becomes nearly linear. In the systems with H_2O–CO_2-fluids, a power law dependence of water solubility on $X^{fl}H_2O$ is observed at $X^{fl}H_2O$<0.3. At higher $X^{fl}H_2O$, the change of the H_2O concentration become less sensitive to changes in the fluid composition for experiments at pressures less than 300 MPa. At 300 and 400 MPa the dependence of H_2O solubility on $X^{fl}H_2O$ is almost linear at $X^{fl}H_2O$>0.3 (Fig. 4a). Moreover, at 500 MPa a point of inflexion in the trend is observed at $X^{fl}H_2O$ ~ 0.5 (Fig. 4a).

The concentrations of CO_2 dissolved in the glass have an almost linear dependence on $X^{fl}CO_2$ at pressures of 50, 100 and 200 MPa (at least within the uncertainty of the data, Fig. 4b). The deviation from linearity increases with pressure. The maximum concentration of CO_2 in basaltic melt were analyzed in glasses coexisting with the most CO_2-rich fluids (for different pressures maximum $X^{fl}CO_2$ varies from 0.7 to 0.9). They vary from about 0.02 wt.% at 50 MPa to 0.33 wt.% at 500 MPa (Table 2). The dependence of CO_2 solubility on pressure can be described as a power function (Fig. 5b).

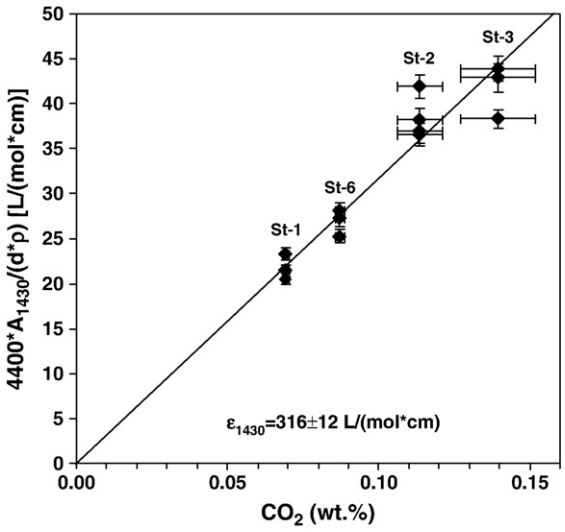

Fig. 3. Calibration plots for the determination of the absorption coefficient for the carbonate band at 1430 cm^{-1}: normalized absorbance of the 1430 cm^{-1} band vs. total carbon content determined by CS analyses (see Sections 2.5 and 3.2).

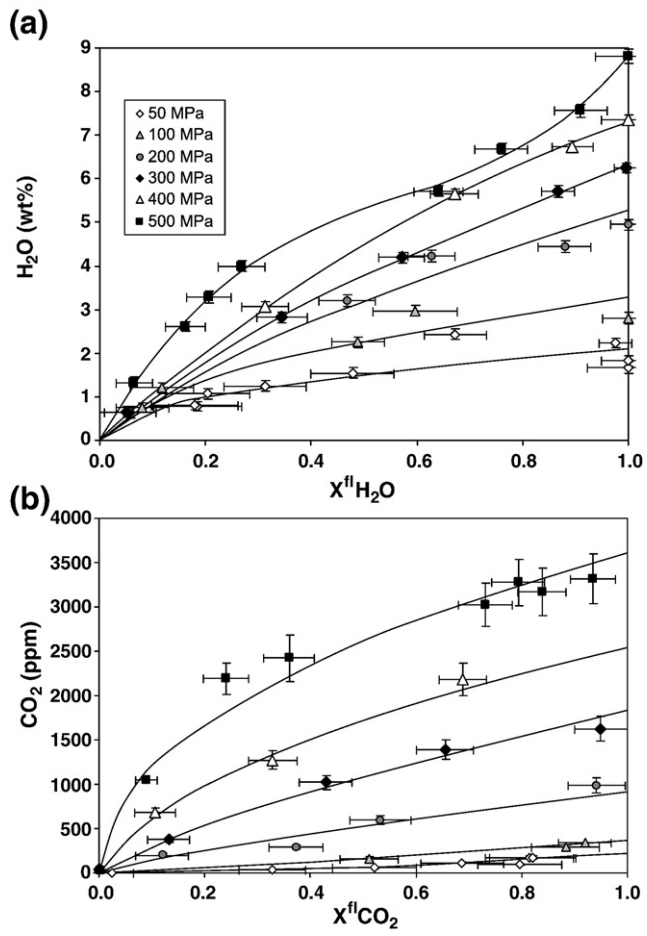

Fig. 4. Relationship between the mole fraction in the fluid phase and the total concentration in the melt for H_2O (a) and CO_2 (b). Dissolved H_2O data are from KFT, CO_2 data from MIR. Solid lines represent trends fitted by power-law for every studied pressure.

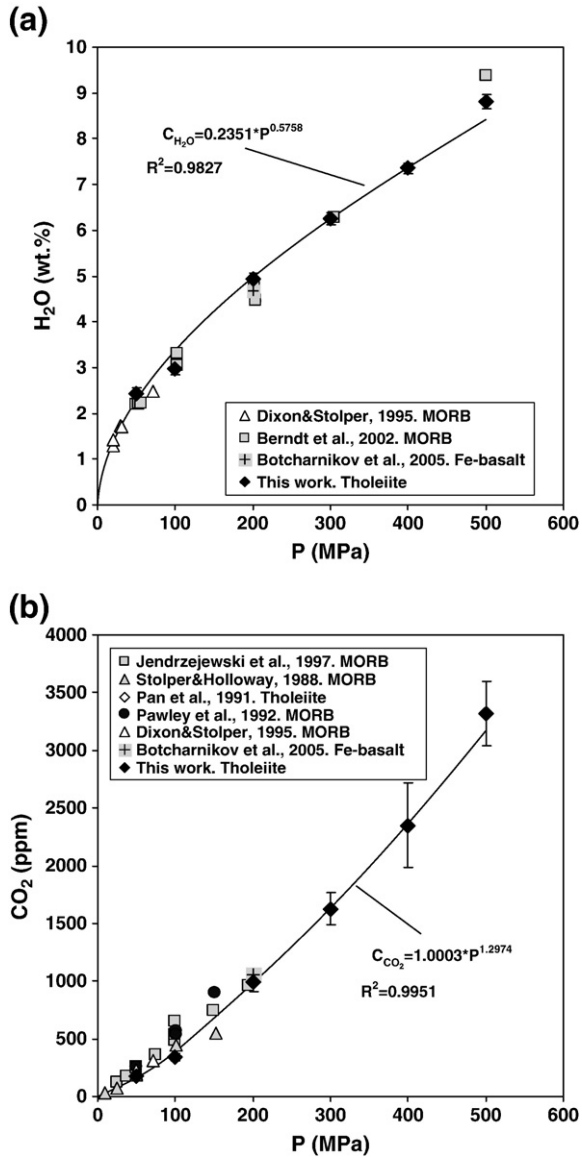

Fig. 5. Solubility of pure H_2O (a) and pure CO_2 (b) in basaltic melts as a function of pressure as determined in this work and from literature data. Power-law equations describe the solubility curves of pure H_2O or CO_2 as function of pressure.

4. Discussion

4.1. Solubility curves in basaltic melts and composition of coexisting fluids

The increase in the concentration of water dissolved in tholeiitic basalt ($X^{fl}H_2O = 1$) with pressure is in a good agreement with recent literature data for other basaltic liquids (Fig. 5a). The plot of water solubility (expressed as wt.% H_2O) as a function of pressure (expressed as MPa) is non-linear at pressures <200 MPa which may be attributed to the predominant solubility of OH groups in silicate melts at low water concentrations (see e.g., Stolper, 1982; Nowak and Behrens, 2001; Liu et al., 2005).

Since all samples contain water in the investigated system, the CO_2 solubility in melts coexisting with pure CO_2-bearing fluids is estimated by the extrapolation of the experimental trends in Fig. 4b towards conditions with $X^{fl}CO_2 = 1$. The estimated solubility of CO_2 increases from 0.02 wt.% at 50 MPa to about 0.33 wt.% at 500 MPa. The trend of CO_2 solubility in the melts as a function of pressure is in a very good agreement with the solubility trends of CO_2 predicted by Holloway and Blank (1994) in basaltic tholeiites up to 500 MPa and with the experimental data for basalts obtained at P<200 MPa (Fig. 5b). The overall agreement with previous datasets indicates that small variations in melt composition (e.g., due to loss of Fe into the capsules observed in our study) do not significantly affect the solubility of CO_2 in basaltic melts.

The solubility of mixed fluids can be illustrated using a conventional diagram with isobaric solubility curves representing the maximum concentrations of CO_2 and H_2O in the silicate melt at a given pressure (solid lines in Fig. 6). The dashed lines in Fig. 6 are isopleths showing the composition of the first fluid that would be in equilibrium with the melt at the onset of degassing. The isobars were plotted by an empirical fit of the experimental data on the H_2O and CO_2 concentrations in the melt. Isopleths with given $X^{fl}H_2O$ were calculated by interpolating the fluid compositions measured in the experiments. It must be noted that these isopleths cannot be extrapolated far beyond the investigated experimental range of pressures. The experimental data plotted in Fig. 6 are helpful for estimating pressures at which magmas might become fluid-saturated and for evaluating the composition of fluids released from the magma, if the concentrations of H_2O and CO_2 in natural basaltic glasses are known. In the next section we compare our experimental results with predictions using the most popular models on H_2O and CO_2 solubility in silicate liquids.

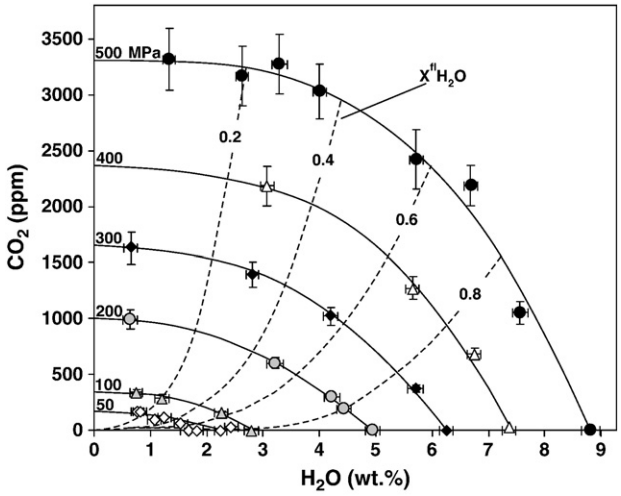

Fig. 6. Solubility plot for H_2O and CO_2 in basaltic melts. The solid lines represent isobars and were drawn by an empirical fit of the experimental data. The dashed lines are isopleths of constant fluid composition for the melts saturated with H_2O–CO_2-bearing fluids calculated by interpolating the fluid compositions measured in the experiments.

4.2. Comparison with numerical models

A detailed description of all available models on H_2O and CO_2 solubility in silicate melts was given in the review paper of Moore (2008). Two models are most widely used for the calculations of H_2O and CO_2 solubilities in basaltic melts: the model of Newman and Lowenstern (2002), known as VolatileCalc, and the model of Papale (1999) which was recalibrated and improved by Papale et al. (2006). VolatileCalc incorporates the regular solution parameters for H_2O solubility determined by Dixon et al. (1995) and uses the CO_2 solubility parameters from Dixon et al. (1995) and Pan et al. (1991). It also includes the compositional parameterization defined by Dixon (1997). This mode of calculation assumes, however, a Henrian behavior of volatile components and does not account for the possible influence of one component on the solubility of the other one. The approach of Papale et al. (2006) is based on the entire experimental dataset for H_2O–CO_2 solubility in silicate liquids available at the time of the code development to calibrate multi-component regular solution model. This model takes into account important parameters such as temperature, pressure, melt composition and, in particular, the effect of the oxidation state of Fe on volatile solubility.

The comparison of experimental data on H_2O and CO_2 solubility in tholeiitic basalt with both the numerical models is illustrated in Fig. 7. The diagrams in Fig. 7 show the relationships between measured and predicted concentrations of H_2O (a) and CO_2 (b) in systems with H_2O- and CO_2-dominated fluids, respectively. The concentrations of dissolved H_2O predicted by the VolatileCalc model are in perfect agreement with the experimental data, whereas the model of Papale et al. (2006) slightly, but systematically, overestimates water solubility in basaltic melts at pressures above 100 MPa (Fig. 7a). The model VolatileCalc reproduces correctly the experimental data on the solubility of CO_2 in basalts coexisting with CO_2-rich fluids (Fig. 7b), but starts to underestimate CO_2 solubility at pressure of 500 MPa (by ~15 relative %). On the other hand, the model of Papale et al. (2006) shows a dramatic overestimation of the CO_2 solubility values. This comparison indicates that the simple approach of ideal behavior of water and carbon dioxide fluids, proposed by Dixon et al. (1995) and developed by Newman and Lowenstern (2002) is successful for basaltic systems coexisting with pure H_2O and pure CO_2 fluids, implying that the small variations in the compositional parameters of the melt (e.g., redox state of Fe) do not have considerable effect for such simple fluid compositions. The discrepancy observed for the second model will be discussed below.

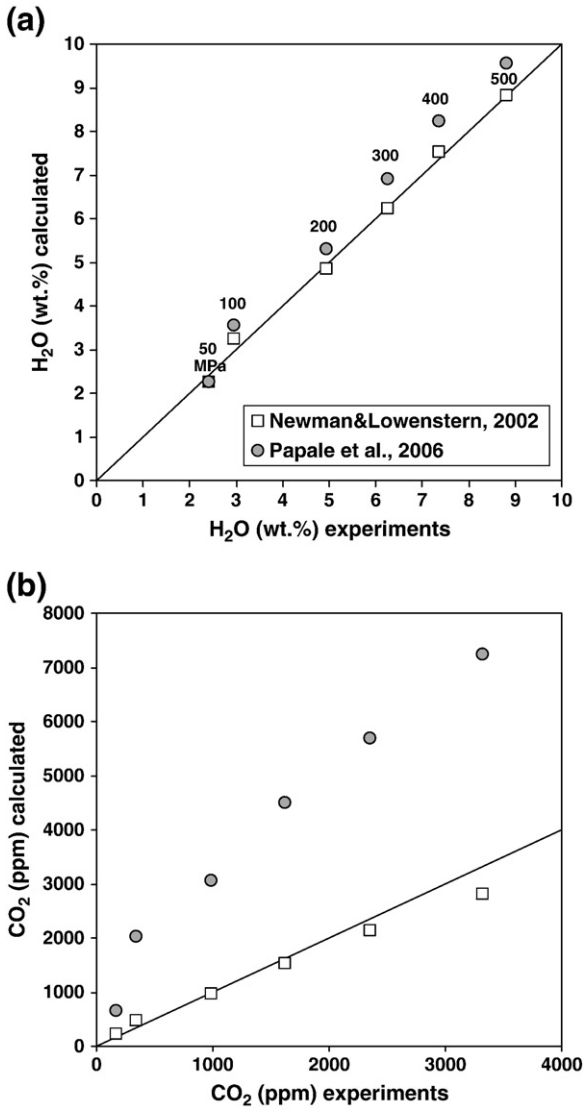

Fig. 7. Comparison of the experimental data on the solubility of pure H_2O (a) and CO_2 (b) in tholeiitic melt with solubilities predicted by numerical models. The solid lines are 1:1 relationships between the experimental and modeled data. Open squares are the data from the model of Newman and Lowenstern (2002), whereas grey circles are the results of the calculations using the model of Papale et al. (2006).

Because the concentrations of dissolved H_2O and CO_2 in the melts equilibrated with mixed fluids depend on many different parameters, it is difficult to compare measured and calculated solubility values. Instead, one can calculate the pressures at which basaltic melts become fluid-saturated for given concentrations of dissolved volatiles and for a given melt composition. Fig. 8 shows the comparison between pressures of the experiments and pressures of fluid saturation calculated using both models (assuming H_2O and CO_2 concentrations determined experimentally). The VolatileCalc model predicts higher pressures for the systems with mixed fluids at P>200 MPa, the difference increases with pressure and may reach about 40 rel.% at 500 MPa. On the contrary, the model of Papale et al. (2006) predicts significantly lower pressures over the entire investigated pressure range and even at 50 and 100 MPa. The observed discrepancy between the experiments and the predictions is presumably attributed to the influence of water on CO_2 solubility which is not properly calibrated in the models. The influence of water on CO_2 solubility in silicate melts has been documented in several studies (e.g., Jakobsson, 1997; Behrens et al., 2004a) and is also illustrated in our dataset at high pressure. For example, at 500 MPa,

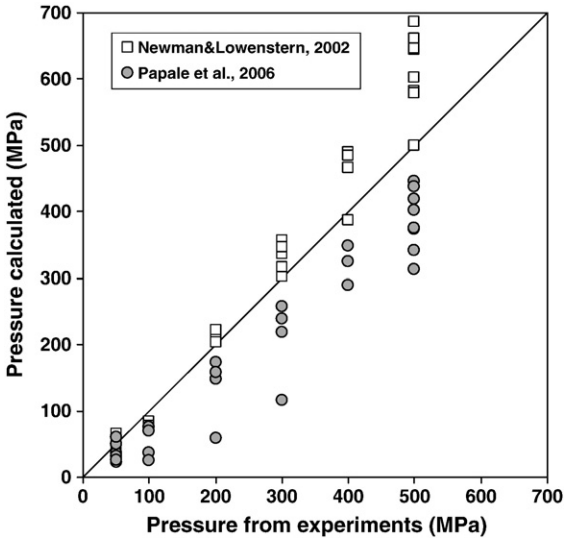

Fig. 8. Comparison between experimental and calculated pressures using the concentrations of dissolved H_2O and CO_2 in the melt. The model of Newman and Lowenstern (2002) significantly overestimates actual pressures at $P>200$ MPa, whereas the model of Papale et al. (2006) underestimates fluid-saturation pressures of the melt in the entire range of investigated pressures.

the maximum CO_2 concentration decreases only slightly with increasing water concentration from 0 to 4 wt.% H_2O. In this water concentration range, the CO_2 solubility is nearly constant within uncertainty with a value of ~3200 ppm (Fig. 6). The same observation was done by Jakobsson (1997) at 1 GPa for an andesitic composition. This behavior possibly results from the effect of dissolved OH groups on the incorporation of CO_2 as proposed in earlier studies (e.g., Mysen et al., 1975; Mysen, 1976; Botcharnikov et al., 2006; Behrens et al., 2009). Thus, the simple assumption of Henrian behavior for the incorporation of water and carbon dioxide in basaltic systems in equilibrium with mixed H_2O- and CO_2-bearing fluids is not valid at least at pressures >200 MPa.

The overestimation of the CO_2 concentrations in basaltic melts (by about 2–3 times for CO_2-rich compositions) using the model of Papale et al. (2006) is related to the limited database for the calibration of the model at pressures above 200 MPa. Moreover, Papale et al. (2006) used only 4 data points from the experiments at 500 MPa for an alkali basalt composition conducted by Freise (2004) and reported by Botcharnikov et al. (2005a). Recently, the basaltic composition studied by Freise (2004) has been re-investigated and we noted that the CO_2 concentrations (reported to be up to 0.7 wt.% CO_2 at 500 MPa) have been overestimated presumably due to a wrong correction factor for the thickness of the samples. The new estimated values for maximum CO_2 content in alkali basalt are in the range from 3500 to 4000 ppm (Botcharnikov et al., 2008) which is consistent with the CO_2 solubility data obtained in this study. Thus, the model of Papale et al. (2006) fails in predicting accurate solubilities at high pressure because no accurate database was available.

The dataset presented in this study is useful to extend the available quantitative models for predicting the degassing conditions of natural basaltic melts up to 500 MPa as it gives systematic information about H_2O–CO_2 solubilities, oxidation state of Fe and changes of the melt composition (Supplementary information, Tables A1, A2).

4.3. Implications for natural systems

As already mentioned above, the volatile solubility diagram shown in Fig. 6 is a powerful tool for the interpretation of volatile concentrations obtained from the natural basaltic melts (quenched matrix glasses, melt inclusions) and especially for the determination of magma storage conditions. Our dataset, obtained only at 1250 °C, needs to be extended to take the effect of temperature into account. However, the temperature effect on H_2O and CO_2 solubility is low in the temperature range from 1100 to 1300 °C (see, for instance, solubility data for andesitic melts obtained by Botcharnikov et al., 2006). Furthermore, strong changes are not expected because tholeiitic melts are not stable at temperatures below 1100 °C (partial crystallization is expected, leading to differentiation of the residual melt). With increasing temperature, the solubility of H_2O in melts coexisting with pure H_2O-bearing fluid decreases slightly at low pressures and increases slightly at high pressures (maximum variations are estimated to be 0.0025 wt.% H_2O/°C in rhyolites; Holtz et al., 1995). Although there is no detailed study on the temperature effect of H_2O-solubility in basaltic melts, the pressure at which H_2O solubility is not dependent on temperature is estimated to be in the range 200–400 MPa. The CO_2 solubility in mafic melts seems to be either independent (e.g., Holloway and Blank, 1994) or only slightly and negatively dependent on temperature (e.g., Botcharnikov et al., 2006 for andesites) indicating that significant temperature correction for the interpretation of melt inclusion or other natural data is not required. Another important aspect is the redox conditions of natural tholeiitic magmas which are typically more reduced than those investigated in this study. The reduction of the magma is expected to have a relatively small effect on the solubility of H_2O (e.g., Berndt et al., 2002; Botcharnikov et al., 2005b), but may presumably lead to changes in CO_2 solubility due to changes in carbon speciation and changes in the Fe redox state in the magma. Furthermore, the increasing proportion of CO over CO_2 in the fluid with reduction of the system will decrease the solubility of CO_2 (e.g., Pawley et al., 1992; Scaillet and Pichavant, 2004; Botcharnikov et al., 2005c). The effect of ferric/ferrous ratio on the solubility of the volatiles is complex and depends on the bulk composition and on the relative proportions of H_2O and CO_2 (according to the model of Papale et al., 2006). Hence, one may expect some deviations in the position of isobars and isopleths in Figs. 6 and 9, but the exact changes remain experimentally unconstrained and require future efforts. It must be noted, however, that our CO_2-rich experiments simulated redox conditions that are relatively close to that of natural magmas (Table 2).

The data are also useful to discuss magmatic processes related with the dynamics of magma evolution and degassing in magma chambers and conduits beneath volcanoes. Fig. 9 shows a compilation of data on volatile concentrations determined in melt inclusions in olivine from low- to mid-K basalts of several geographical and geological localities:

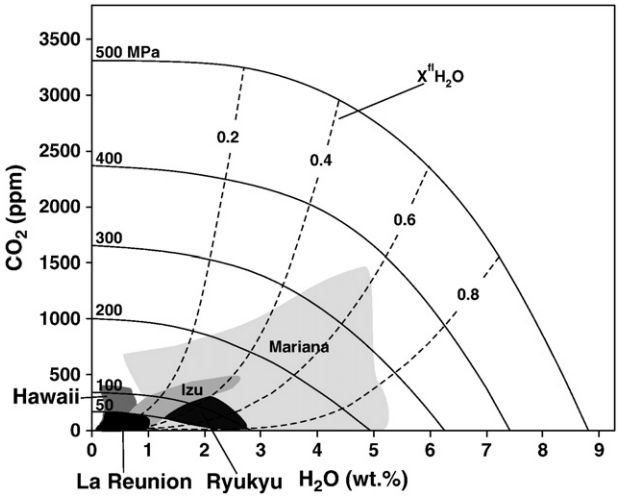

Fig. 9. Comparison of the experimental data with the concentrations of H_2O and CO_2 measured in melt inclusions hosted in olivines from low- to mid-K tholeiitic basalts from different localities: Mariana arc (Newman et al., 2000; Shaw et al., 2008), Ryukyu arc (Saito et al., 2001), Izu arc (Nichols and Wysoczanski, 2007), Hawaii (Harris and Anderson, 1983; Anderson and Brown, 1993), La Reunion (Famin et al., 2009).

Hawaii (Harris and Anderson, 1983; Anderson and Brown, 1993), Mariana arc (Newman et al., 2000; Shaw et al., 2008), Ryukyu arc (Saito et al., 2001), Izu arc (Nichols and Wysoczanski, 2007), Reunion (Famin et al., 2009). The measured compositional values are compared with the experimental isobars and isopleths for basaltic melts saturated with respect to H_2O- and CO_2-bearing fluids. All reported values indicate that the melts were saturated with respect to fluids at pressures lower than 400 MPa. Assuming that melt inclusions did not exchange volatiles with the surrounding magma during magma evolution (no gain or loss), this observation indicates that most melt inclusions were trapped in olivines at relatively shallow levels in magmatic systems of the Mariana arc (<12–15 km) and at very shallow levels for the other examples (<5–6 km). The compositional trends for the different magmatic suites also clearly reflect different evolution and degassing histories of natural magmas, depending on their geodynamic setting. As expected, the subduction-related magmas show systematically higher H_2O proportions, but the pressure at which the melt inclusions may become saturated with respect to fluids is in the same range for Hawaii, Ryukyu arc and Izu arc.

5. Conclusion

Based on our experimental data combined with previous datasets, a quantitative evaluation of the storage conditions and degassing paths of tholeiitic magmas can be achieved up to 500 MPa. The experimental data on H_2O and CO_2 solubility in tholeiitic melts show that models neglecting the interactions between H_2O- and CO_2-bearing species (e.g., VolatileCalc; Newman and Lowenstern, 2002) are successful up to 200 MPa but that they do not predict accurately the volatile solubilities at pressures above 200 MPa. The deviation from such models increases with increasing pressure. Our dataset, obtained only at 1250 °C, needs to be extended to take the effect of temperature into account. The new experimental data can be used to improve the existing numerical models on H_2O–CO_2 solubility in basaltic melts and to provide more accurate constraints on the pressure conditions of magma storage, fractionation and degassing.

Supplementary materials related to this article can be found online at doi:10.1016/j.chemgeo.2010.07.014.

Acknowledgements

We thank H. Behrens for his advises, O. Diedrich for preparation of samples for infra-red spectroscopy and microprobe analyses, A. Wegorzewski for determinations of redox state of Fe. We appreciate two anonymous reviewers for their constructive comments of the manuscript. This research has been supported by the German Science Foundation (DFG project Ho1337/21) and by the Russian-German project KALMAR funded by BMBF.

References

Anderson Jr., A.T., Brown, G.G., 1993. CO_2 contents and formation pressures of some Kilauean melt inclusions. American Mineralogist 78, 794–803.

Aranovich, L.Y., Newton, R.C., 1999. Experimental determination of CO_2-H_2O activity-concentration relations at 600–1000 C and 6–14 kbar by reversed decarbonation and dehydration reactions. American Mineralogist 84, 1319–1332.

Behrens, H., Romano, C., Nowak, M., Holtz, F., Dingwell, D.B., 1996. Near-infrared spectroscopic determination of water species in glasses of system $MAlSi_3O_8$ (M = Li, Na, K): an interlaboratory study. Chemical Geology 128, 41–63.

Behrens, H., Ohlhorst, S., Holtz, F., Champenois, M., 2004a. CO_2 solubility in dacitic melts equilibrated with H_2O–CO_2 fluids – implications for modelling the solubility of CO_2 in silicic melts. Geochimica et Cosmochimica Acta 68, 4687–4703.

Behrens, H., Zhang, Y., Xu, Z., 2004b. H_2O diffusion in dacitic and andesitic melts. Geochimica et Cosmochimica Acta 68, 5139–5150.

Behrens, H., Misiti, V., Freda, C., Vetere, F., Botcharnikov, R.E., Scarlato, P., 2009. Solubility of H_2O and CO_2 in ultrapotassic melts at 1200 and 1250 °C and pressure from 50 to 500 MPa. American Mineralogist 94, 105–120.

Berndt, J., Liebske, C., Holtz, F., Freise, M., Nowak, M., Ziegenbein, D., Hurkuck, W., Koepke, J., 2002. A combined rapid-quench and H_2-membrane setup for internally heated pressure vessels: description and application for water solubility in basaltic melts. American Mineralogist 87, 1717–1726.

Blank, J.G., Brooker, R.A., 1994. Experimental studies of carbon dioxide in silicate melts: solubility, speciation, and stable carbon isotope behavior. In: Carrol, M.R., Holloway, J.R. (Eds.), Reviews in Mineralogy, 30, pp. 157–186.

Blank, J.G., Stolper, E.M., Carrol, M.R., 1993. Solubilities of carbon dioxide and water in rhyolitic melt at 850 °C and 750 bars. Earth and Planetary Science Letters 119, 27–36.

Botcharnikov, R.E., Freise, M., Holtz, F., Behrens, H., 2005a. Solubility of C–O–H mixtures in natural melts: new experimental data and application range of recent models. Annals of Geophysics 48, 633–646.

Botcharnikov, R.E., Koepke, J., Holtz, F., McCammon, C., Wilke, M., 2005b. The effect of water activity on the oxidation and structural state of Fe in a ferro-basaltic melt. Geochimica et Cosmochimica Acta 69, 5071–5085.

Botcharnikov, R.E., Holtz, F., Behrens, H., Freise, M., 2005c. The effect of redox state on the solubility of C–O–H fluids in silicate melts: new experimental evidences. Geophysical Research Abstracts 7, 09237.

Botcharnikov, R.E., Behrens, H., Holtz, F., 2006. Solubility and speciation of C–O–H fluids in andesitic melt at $T = 1100$–1300 °C and $P = 200$ and 500 MPa. Chemical Geology 229, 125–143.

Botcharnikov, R.E., Almeev, R.R., Holtz, F., Behrens, H., 2008. Solubility of C–O–H fluids in mafic melts at 500 MPa. Abs. IAVCEI meeting 2008, General assembly, Reykjavik, Iceland.

Dixon, J.E., 1997. Degassing of alkali basalts. American Mineralogist 82, 368–378.

Dixon, E.J., Stolper, E.M., Holloway, J.R., 1995. An experimental study of water and carbon dioxide solubilities in mid-ocean ridge basaltic liquids. Part 1: Calibration and solubility models. Journal of Petrology 36, 1607–1631.

Duggen, S., Portnyagin, M.V., Baker, J., Ulfbeck, D., Hoernle, K., Garbe-Schonberg, D., Grassineau, N., 2007. Drastic shift in lava geochemistry in the volcanic-front to rear-arc region of the Southern Kamchatkan subduction zone: evidence for the transition from slab surface dehydration to sediment melting. Geochimica et Cosmochimica Acta 71, 452–480.

Famin, V., Welsch, B., Okumura, S., Bachelery, P., Nakashima, S., 2009. Three differentiation stages of a single magma at Piton de la Fournaise volcano (Reunion hot spot). Geochemistry, Geophysics, Geosystems 10, Q01007.

Fine, G., Stolper, E., 1986. Carbon dioxide in basaltic glasses: concentrations and speciation. Earth and Planetary Science Letters 76, 263–278.

Fischer, T.P., Marty, B., 2005. Volatile abundances in the sub-arc mantle: insights from volcanic and hydrothermal gas discharges. Journal of Volcanology and Geothermal Research 140, 205–216.

Freise, M., 2004. Differenzierung von Basalten einer "Large Igneous Province" am Beispiel des Kerguelen Plateaus. Eine experimentelle Studie. PhD thesis, University of Hannover.

Giggenbach, W.F., 1996. Chemical composition of volcanic gases. In: Scarpa, R., Tilling, R.I. (Eds.), Monitoring and Mitigation of Volcanic Hazards. Springer, Berlin, pp. 221–256.

Harris, D.M., Anderson Jr., A.T., 1983. Concentrations, sources, and losses of H_2O, CO_2, and S in Kilauean basalt. Geochimica et Cosmochimica Acta 47, 1139–1150.

Holloway, J.R., Blank, J.G., 1994. Application of experimental results to C–O–H species in natural melts. In: Carrol, M.R., Holloway, J.R. (Eds.), Reviews in Mineralogy, 30, pp. 187–230.

Holtz, F., Behrens, H., Dingwell, D.B., Johannes, W., 1995. Water solubility in haplogranitic melts. Compositional, pressure and temperature dependence. American Mineralogist 80, 94–108.

Jakobsson, S., 1997. Solubility of water and carbon dioxide in an icelandite at 1400 °C and 10 kilobars. Contributions to Mineralogy and Petrology 127, 129–315.

King, P.L., Holloway, J.R., 2002. CO_2 solubility and speciation in intermediate (andesitic) melts: the role of H_2O and composition. Geochimica et Cosmochimica Acta 66, 1627–1640.

Liu, Y., Zhang, Y., Behrens, H., 2005. Solubility of H_2O in rhyolitic melts at low pressures and a new empirical model for mixed H_2O–CO_2 solubility in rhyolitic melts. Journal of Volcanology and Geothermal Research 143, 219–235.

Mandeville, C.W., Webster, J.D., Rutherford, M.J., Taylor, B.E., Timbal, A., Faure, K., 2002. Determination of molar absorptivities for infrared absorption bands of H_2O in andesitic glasses. American Mineralogist 87, 813–821.

Martynov, Y.A., Chashchin, A., 1989. Rock-forming minerals of the mafic effusives of Mutnovsky geothermal field. New data on petrology of the magmatic and metamorfic rocks in Kamchatka. FarEast Branch, USSR Academy of Science, Vladivostok, pp. 112–123 (in Russian).

Martynov, Y.A., Perepelov, A.B., Chashchin, A., 1995. Geochemical typization of the basaltoids from Mutnovsky volcani field (Southern Kamchatka). Geology of the Pacific Ocean (Tikhookeanskaya Geologiya) 5, 72–83 (in Russian).

Moore, G., 2008. Interpreting H_2O and CO_2 contents in melt inclusions. Constraints from Solubility Experiments and Modeling Reviews in Mineralogy and Geochemistry 69, 333–362.

Mysen, B.O., 1976. The role of volatiles in silicate melts; solubility of carbon dioxide and water in feldspar, pyroxene, and feldspathoid melts to 30 kb and 1625 degrees C. American Journal of Science 276, 969–996.

Mysen, B.O., Arculus, R.J., Eggler, D.H., 1975. Solubility of carbon dioxide in natural nephelinite, tholeiite, and andesite melt to 30 kbar pressure. Contributions to Mineralalogy and Petrology 53, 227–239.

Newman, S., Lowenstern, J.B., 2002. VolatileCalc: a silicate melt-H_2O–CO_2 solution model written in Visual Basic for Excel. Computers & Geosciences 28, 597–604.

Newman, S., Stolper, Ed., Stern, R., 2000. H_2O and CO_2 in magmas from the Mariana arc and back arc systems. Geochemistry, Geophysics, Geosystems 1 30 pp..

Nichols, A.R.L., Wysoczanski, R.J., 2007. Using micro-FTIR spectroscopy to measure volatile contents in small and unexposed inclusions hosted in olivine crystals. Chemical Geology 242, 371–384.

Nowak, M., Behrens, H., 2001. Water in rhyolitic magmas: getting a grip on a slippery problem. Earth Planetary Science Letters 184, 515–522.
Ohlhorst, S., Behrens, H., Holtz, F., 2001. Compositional dependence of molar absorptivities of near-infrared OH- and H_2O bands in rhyolitic to basaltic glasses. Chemical Geology 174, 5–20.
Pan, V., Holloway, J.R., Hervig, R.L., 1991. The pressure and temperature dependence of carbon dioxide solubility in tholeiitic basalt melts. Geochimica et Cosmochimica Acta 55, 1587–1595.
Papale, P., 1999. Modeling of the solubility of a two-component $H_2O + CO_2$ fluid in silicate liquids. American Mineralogist 84, 477–492.
Papale, P., Moretti, R., Barbato, D., 2006. The compositional dependence of the saturation surface of $H_2O + CO_2$ fluids in silicate melts. Chemical Geology 229, 78–95.
Pawley, A.R., Holloway, J.R., McMillan, P.F., 1992. The effect of oxygen fugacity on the solubility of carbon-oxygen fluids in basaltic melt. Earth and Planetary Science Letters 110 (1–4), 213–225.
Pineau, F., Semet, M.P., Grassineaua, N., Okrugin, V.M., Javoy, M., 1999. The genesis of the stable isotope (O, H) record in arc magmas: the Kamtchatka's case. Chemical Geology 153, 93–124.
Pitzer, K.S., Sterner, S.M., 1994. Equation of state valid continuously from zero to extreme pressures for H_2O and CO_2. Journal of Chemistry and Physics 102, 3111–3116.
Richet, P., Whittington, A., Holtz, F., Behrens, H., Ohlhorst, S., Wilke, M., 2000. Water and density of silicate glasses. Contribution to Mineralogy and Petrology 138, 337–347.
Saito, G., Kazahaya, K., Shinohara, H., Stimac, J., Kawanabe, Y., 2001. Variation of volatile concentration in a magma system of Satsuma–Iwojima volcano deduced from melt inclusions analyses. Journal of Volcanology and Geothermal Research 108, 11–31.
Scaillet, B., Pichavant, M., 2004. Role of fO_2 on fluid saturation in oceanic basalt. Nature 430 (6999).
Schuessler, J.A., Botcharnikov, R.E., Behrens, H., Misiti, V., Freda, C., 2008. Oxidation state of iron in hydrous phono-tephritic melts. American Mineralogist 93, 1493–1504.
Shaw, A.M., Hauri, E.H., Fischer, T.P., Hilton, D.R., Kelley, K.A., 2008. Hydrogen isotopes in Mariana arc melt inclusions: implications for subduction dehydration and the deep-Earth water cycle. Earth Planetary Science Letters 275, 138–145.
Sisson, T.W., Layne, G.D., 1993. H_2O in basalt and basaltic andesite glass inclusions from four subduction-related volcanoes. Earth and Planetary Science Letters 117, 619–635.
Stolper, E., 1982. The speciation of water in silicate melts. Geochimica et Cosmochimica Acta 46, 2609–2620.
Symonds, R.B., Rose, W.I., Bluth, G.J.S., Gerlach, T.M., 1994. Volcanic-gas studies; methods, results, and applications. In: Carroll, M.R., Holloway, J.R. (Eds.), Reviews in Mineralogy, 30. Mineralogical Society of America, Washington, pp. 1–66.
Tamic, N., Behrens, H., Holtz, F., 2001. The solubility of H_2O and CO_2 in rhyolitic melts in equilibrium with a mixed CO_2-H_2O fluid phase. Chemical Geology 174, 333–347.
Wallace, P.J., 2005. Volatiles in subduction zone magmas: concentrations and fluxes based on melt inclusion and volcanic gas data. Journal of Volcanology and Geothermal Research 140, 217–240.
Wilson, A.D., 1960. The micro-determination of ferrous iron in silicate minerals by a volumetric and colorimetric method. Analyst 85, 823–827.